Digestive Diseases and Sciences, Vol. 43, No. 6 (June 1998), pp. 1193–1199

Optical Biopsy in Human Pancreatobiliary Tissue Using Optical Coherence Tomography

G.J. TEARNEY, PhD, M.E. BREZINSKI, MD, PhD, J.F. SOUTHERN, MD, B.E. BOUMA, PhD, S.A. BOPPART, MS, and J.G. FUJIMOTO, PhD

Optical coherence tomography (OCT) is a new technique for performing high-resolution, cross-sectional tomographic imaging in human tissue. OCT is analogous to ultrasound B mode imaging except that it uses light rather than acoustical waves. As a result, OCT has over 10 times the resolution of currently available clinical high-resolution cross-sectional imaging technologies. In this work, we investigate the capability of OCT to differentiate the architectural morphology of pancreatobiliary tissues. Normal pancreatobiliary tissues, including the gallbladder, common bile duct, pancreatic duct, and pancreas were taken postmortem and imaged using OCT. Images were compared to corresponding histology to confirm tissue identity. Microstructure was delineated in different tissues, including tissue layers, glands, submucosal microvasculature, and pancreatic islets of Langerhans. The ability of OCT to provide high-resolution imaging of pancreatobiliary architectural morphology suggests the feasibility of using OCT as a powerful diagnostic endoscopic imaging technology to image early stages of pancreatobiliary disease.

KEY WORDS: optical coherence tomography; optical biopsy; microscopy; imaging; pancreatobiliary tissue.

Recently, high-frequency ultrasound transducers have been attached to the distal portions of endoscopes with the objective of improving the resolution available for clinical diagnostics (1–5). An imaging technology that can yield resolutions in the micron range can provide information on tissue microstructure that could only previously be obtained with conventional excisional biopsy. In this paper, we present a recently developed optical imaging technique, optical coherence tomography (OCT), for obtaining high-resolution, cross-sectional images or optical biopsies of pancreatobiliary tissues.

OCT is similar to B mode ultrasound imaging except that it measures reflected infrared light rather than acoustical waves (6). The intensity of reflected light from structures within tissue is displayed as a function of depth. Tomographic images are produced by scanning the optical beam across the sample and generating two dimensional data. Thus, an OCT image represents a cross-sectional depiction of the optical reflectance within tissue.

OCT was initially introduced to image the trans-

Manuscript received July 25, 1997; revised manuscript received January 15, 1998; accepted February 23, 1998.

From the Harvard Medical School and Cardiac Unit, Massachusetts General Hospital, Boston, Massachusetts 02114; and Department of Electrical Engineering and Computer Science, and Research Laboratory of Electronics, Massachusetts Institute of Technology, Cambridge, Massachusetts 02139.

This research is supported in part by grants from the National Institutes of Health, contracts NIH-9-RO1-EY11289-11 (to J.G.F.), NIH-1-R01-CA75289-01 (to J.G.F. and M.E.B.), NIH-1-R29-HL55686-01A1 (to M.E.B.), NIH-RO1-AR44812-01 (to M.E.B.), the Office of Naval Research, Medical Free Electron Laser Program, grant N000014-97-1-1066, and the Whittaker Foundation contract 96-0205 (to M.E.B.).

Address for reprint requests: James G. Fujimoto, Massachusetts Institute of Technology, Building 36-357, 77 Massachusetts Avenue, Cambridge, Massachusetts 02139.

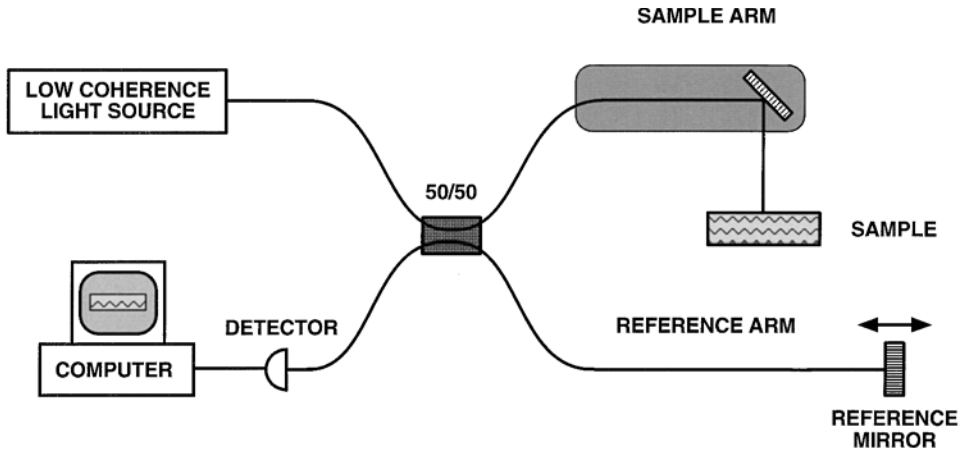

Fig 1. Schematic of the OCT system. Infrared light generated from the low coherence source is split evenly, half to the sample and half toward a moving mirror. Light is reflected off the reference mirror and from within the sample and recombined in the beam splitter (50/50). If the light reflected from within the sample travels the same distance (optical) as light from the reference mirror, interference will occur at the detector. OCT measures the intensity of this interference, which represents the intensity of back-reflection. Moving the mirror changes the distance traveled by light in the reference arm, allowing back-reflecting intensity to be assessed at different depths within the tissue. The back-reflecting intensity is plotted as a function of depth analogous to conventional ultrasound imaging. The shaded area represents the portion of the system that would be present within the endoscope, consisting primarily of an optical fiber, lens, and mirror.

parent tissue of the eye and is currently being used in clinical trials to diagnose retinal macular disease (7, 8). Although application of OCT in tissues that are nontransparent and scatter light is more challenging, imaging in nontransparent tissue has been achieved by using longer wavelengths in the near-infrared, taking advantage of the decreased scattering of light at these wavelengths (9–14). While the imaging depth of OCT in scattering tissues is limited to a few millimeters, the resolution of this optical technology is approximately 10 times higher than clinical high-frequency ultrasound, the currently available technology with the highest resolution for cross-sectional endoluminal imaging.

The goal of this study was to investigate the feasibility of using OCT for high resolution intraluminal imaging of the pancreatobiliary system. To accomplish this, OCT images of pancreatobiliary tissues were acquired *in vitro* and correlated with histology. The results demonstrate the capability of this technique to allow acquisition of optical biopsies of pancreatobiliary tissue microstructure. In particular, the high resolution of OCT and its ability to be easily incorporated into fiberoptic endoscopes make it an attractive technology for the microstructural diagnosis of pancreatobiliary disease.

MATERIALS AND METHODS

OCT is analogous to ultrasound except that it uses light rather than acoustical waves. Ultrasound imaging is accomplished by measuring the delay time (echo delay) for an incident ultrasonic pulse to be reflected back from structures within tissue. Relative to light, the velocity of sound is slow, and thus the echo delay time can be measured electronically. However, since the velocity of light is approximately 10^6 times greater than sound, OCT measurements of delay time, unlike ultrasound, cannot be performed easily using standard electronic detection. Therefore, a technique known as low coherence interferometry is used to measure the delay time of reflected light from within tissue (15). Low coherence interferomety functions by comparing light reflected from internal microstructures in the tissue specimen to light traversing a reference path of known path length.

Figure 1 shows a schematic of the OCT system. Low coherence light, which can be envisioned for illustrative purposes as pulses, is generated from the source. The light is split evenly, using a fiberoptic beamsplitter. Half the light is directed toward the sample and half toward a moving mirror. The light is then reflected both from within the sample and from the mirror. If the distance traveled by pulses in both arms is nearly identical, interference will occur when the light reflected from the sample and the light reflected from the reference arm mirror recombine at the beam splitter. More specifically, interference will occur if the two path lengths are matched to within the property of light known as the coherence length, which is analogous to the pulse duration.

Axial scans of reflected light from within the tissue are obtained by changing the position of the moving reference mirror. By moving the mirror, the distance light travels in the reference arm is changed, which allows interference information from different depths within the tissue to be recorded. The magnitude of the interference, proportional to the reflected or backscattered light from structures inside tissue, is then plotted as a function of depth in a manner similar to A mode ultrasound. A cross-sectional image is created by acquiring multiple axial scans as the beam position is scanned across the sample. The resulting data are displayed as a grey scale or false color image. The image contrast in an OCT image arises from variations in the optical reflectance of the tissue.

Both a superluminescent diode light source (which is similar in some respects to sources used in compact disc players) and a femtosecond solid-state laser (generating pulses of 10^{-14} sec in duration) were used for imaging. The diode had a median wavelength of 1300 nm and a spectral bandwidth of 50 nm, while the laser had a median wavelength of 1280 nm and a bandwidth of 130 nm. The bandwidth, $\Delta\lambda$, is defined by the wavelength distribution of the source. It is inversely related to the coherence length or the axial resolution of the OCT system, Δz, via the formula (15):

$$\Delta z = \frac{2\ln 2}{\pi} \frac{\lambda^2}{\Delta\lambda} \quad (1)$$

The axial resolution of the OCT images acquired in this study was either 15 μm for the superluminescent diode or 5 μm for the solid state laser source. The axial resolution was determined experimentally by measuring the point spread function using a mirror in the sample arm of the interferometer (13). A lateral resolution of 20 μm was determined by measuring the spot size on the sample. In general, both the lateral and axial resolutions for OCT were approximately 10× higher than EUS and 10× lower than conventional high power microscopy. The incident power on the sample ranged from 150 μW to 1 mW, which provided a signal-to-noise ratio greater than 110 dB. The dimensions of the OCT images in this study were 3 (axial) × 6 (transverse) mm, which corresponded to 250 (axial) × 500 (transverse) pixels. The image acquisition time was 45 sec, but systems have recently been developed that can now image at 4–8 frames/sec (16).

Normal pancreatobiliary tissues were obtained within 5 hr of the initiation of autopsy. More than 20 different samples from five patients were examined. The tissue samples were placed in isotonic saline with 0.05% sodium azide and stored at 0°C. The tissues were dissected to dimensions of approximately 10 × 5 mm and imaged with the luminal surfaces exposed. During imaging, the tissues were partially immersed in isotonic saline to prevent dehydration. The saline did not cover the surface of the tissue.

Imaging was performed through air at room temperature. The position of the beam on the sample was monitored using a visible light guiding beam (633 nm helium neon laser) that was coincident with the 1300-nm infrared OCT beam on the sample. The imaging planes were marked using small injections of dye. The samples then underwent routine histologic processing. Samples were immersed in 10% buffered formalin for 48 hr, and the tissues were then processed for standard paraffin embedding. Five-micron-thick sections were cut at the marked imaging sites and stained with hematoxylin and eosin (H&E) or trichrome blue. The stained histologic sections enabled verification of tissue identity and, in most instances, allowed identification of sources of tissue contrast in the OCT images.

RESULTS

Gallbladder. It is possible to differentiate several anatomic layers of the gallbladder in the OCT image, including the mucosa–submucosa, muscularis, and serosa (Figure 2). Villi on the surface of the OCT image can be clearly visualized. These outpocketings of tissue represent the columnar epithelium and lamina propria of the mucosa of the gallbladder. Diverticula or infoldings of the mucosa can also be seen at the surface of the OCT image. Vascular structures in the submucosa and muscularis can also be identified in the image. Areas of relatively low backscatter in the serosa represent the presence of adipose tissue, which has been previously demonstrated to have a low reflection intensity in OCT imaging (13).

Common Bile Duct. OCT images of the layered common bile duct also demonstrate the capability of OCT to resolve the submucosa–muscularis and muscularis–adventitia boundaries (Figure 3). Differentiation of the submucosa, muscularis, and adventitial layers is made possible by visualization of the different backscattering characteristics within each layer. The adventitial layer seems to have a lower and more irregular backscattering intensity than the submucosa or muscularis. This irregular backscattering pattern is most likely due to the presence of adipose tissue in the adventitial layer. The high resolution of OCT enables tissue microstructure, such as secretions within individual glands, to be visualized (Figure 3). In addition, invagination of gland ducts from the mucosal surface can be identified in the submucosa (Figure 3). Histology is provided only to confirm tissue identification.

Pancreatic Duct. In the pancreatic duct, the dense connective tissue layer containing elastic fibers is well differentiated from the underlying pancreas (Figure 4). Adipose tissue is clearly distinguishable from both the stroma of the pancreas and the connective tissue beneath the epithelium. The outlines of entire subepithelial adipose cells can be visualized in the OCT image of the pancreatic duct.

Islets of Langerhans. High-resolution OCT imaging using the solid-state laser source enables cross-sectional imaging of islets of Langerhans cells. In

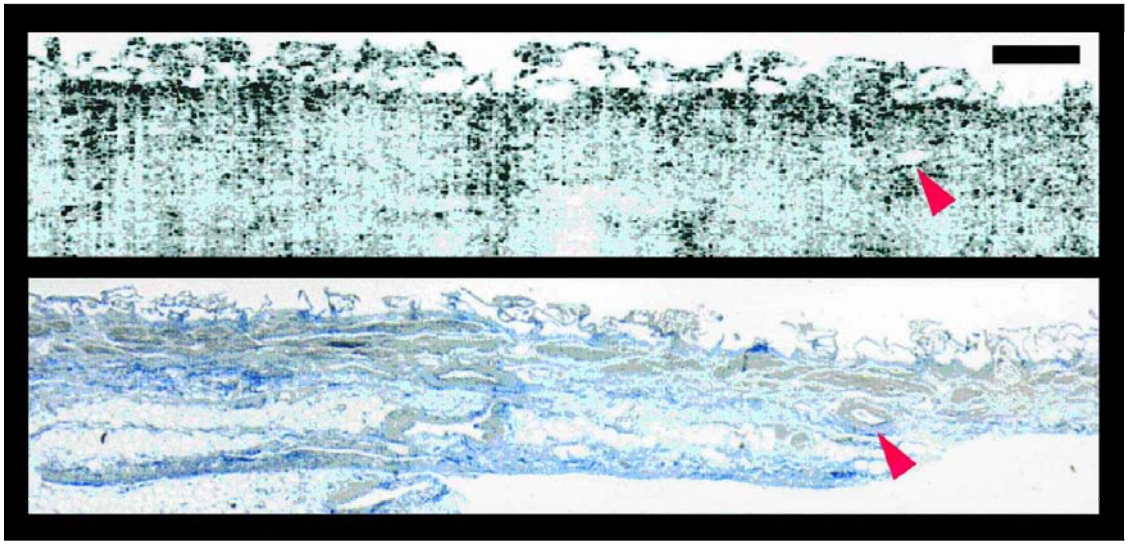

Fig 2. Gallbladder. The submucosa, muscularis, and serosa can be visualized in the OCT image. Arrows point to a small muscular artery in the muscularis. Corresponding histology (trichrome blue) has been provided. The axial resolution, Δz, of this image is 15 μm. Scale bar, 500 μm.

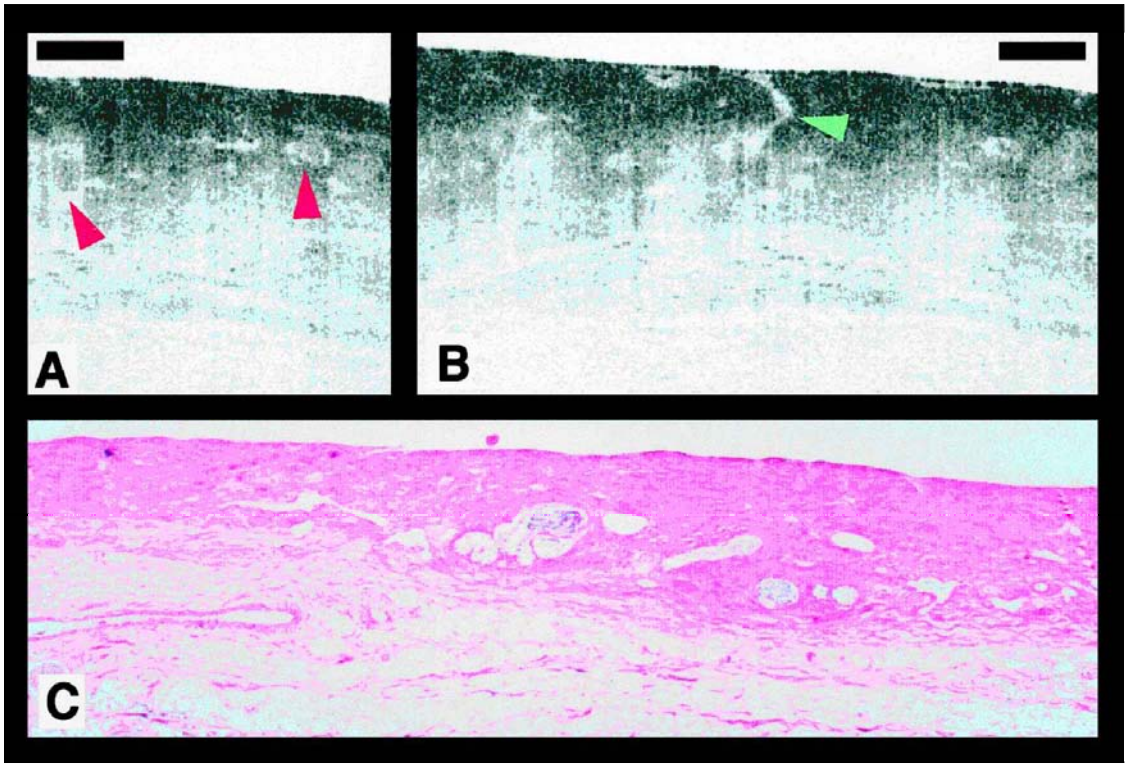

Fig 3. Common bile duct. (A) Red arrows show glands containing secretions in the submucosa. (B) Green arrow points to a duct invaginating from the luminal surface. The submucosa, muscularis, and adventitia are identifiable as layers with different backreflection characteristics in both OCT images. (C) The histology (H&E) has been provided only for tissue identification and not correspondence. The axial resolutions, Δz, of A and B are 15 μm. Scale bars, 500 μm.

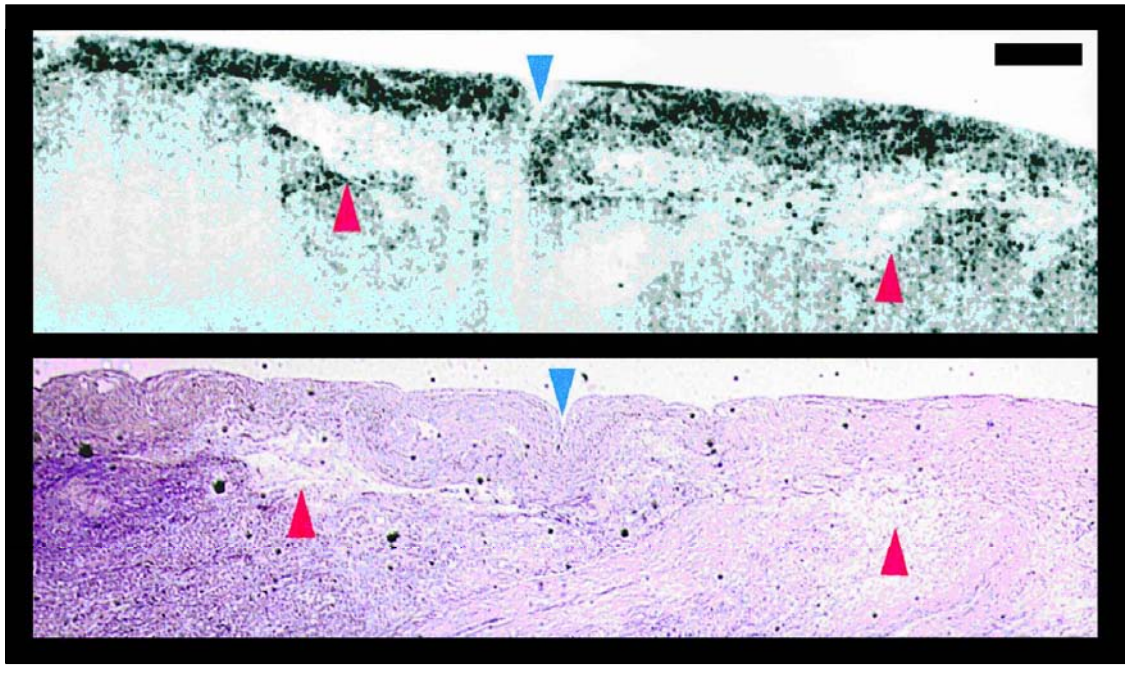

Fig 4. Pancreatic duct. The arrows point to corresponding locations in the OCT and histology (trichrome blue) images. Red arrows point to adipose tissue underlying the collagenous layers of the pancreatic duct, while the blue arrow identifies the duct. The axial resolution, Δz, of this image is 15 μm. Scale bar, 500 μm.

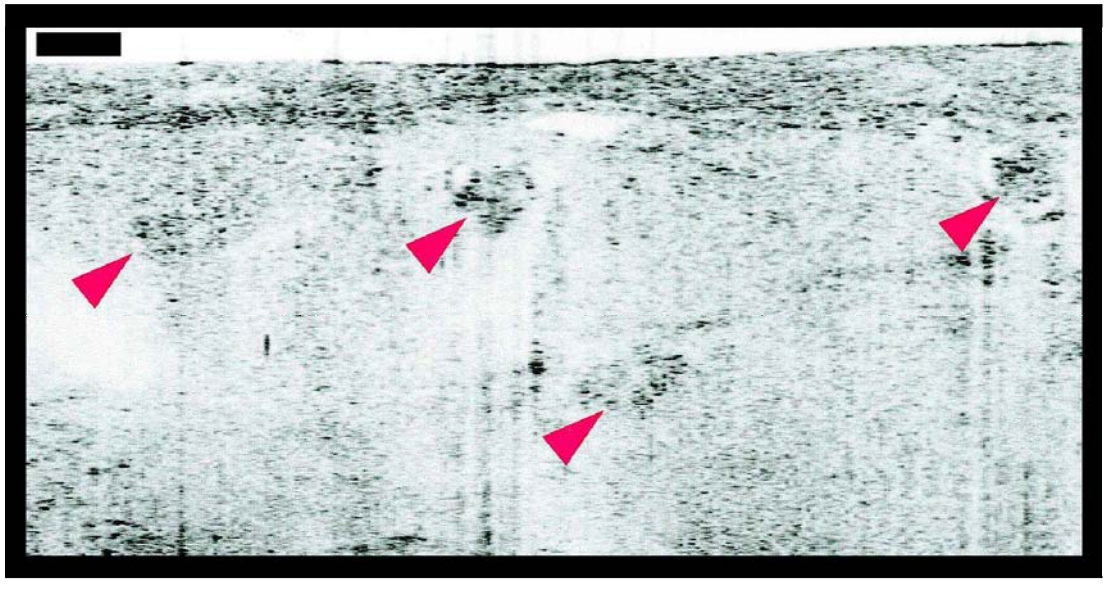

Fig 5. Islets of Langerhans. The OCT image demonstrates islets of Langerhans within the pancreas, beneath the pancreatic duct (arrows). Islet cells are highly reflective relative to the surrounding pancreatic stroma. The axial resolution, Δz, of this image is 5 μm. Scale bar, 150 μm.

Figure 5, the pancreatic duct appears as a highly backscattering band near the lumen of the tissue. Pancreatic stroma can be seen beneath the pancreatic duct. Several islets of Langerhans, each approximately 150 μm in diameter, can be clearly visualized as highly back-reflecting rings within the normal glandular tissue stroma.

DISCUSSION

OCT has the potential to allow the endoscopist to delineate tissue microstructure *in situ* and in real time at an axial resolution not available with current imaging technologies. In this work, the ability of OCT to resolve tissue architectural morphology was demonstrated with both a superluminescent diode and a solid-state laser source. While the superluminescent diode yields a lower axial resolution (15 μm) than the solid-state laser source (5 μm), it is compact, stable, and inexpensive. Although broad bandwidth solid-state lasers generate resolutions near the cellular level, with some systems in the range of μm, they are not clinically viable sources due to their complexity (17). However, compact, inexpensive sources with similar wavelength characteristics are under development that will likely allow cellular level imaging in the clinical setting.

Since OCT is based on light rather than sound, imaging is possible through air and does not require a transducing medium or direct contact with the tissue surface. Therefore, the use of an imaging balloon or saline injections, which can lead to impractical time demands on the gastroenterologist, is not necessary. Moreover, OCT images are not degraded by optically transparent media such as saline or saliva between the endoscope and the tissue. However, scattering debris between the endoscope and the tissue will degrade the OCT image and potentially may cause shadowing artifacts similar to those commonly seen in ultrasound.

Since OCT is based on technology used in fiberoptic communication, its integration into endoscopes is straightforward. An electronic transducer is not required at the distal end of the endoscope because light can be transmitted bidirectionally through optical fibers that are small and flexible. In future studies, a recently developed 1-mm-diameter OCT imaging endoscope will be used for performing OCT imaging of *in vivo* pancreatobiliary tissues (18).

In conclusion, high-resolution, cross-sectional OCT images of *in vitro* pancreatobiliary tissues have been acquired and correlated with conventional histopathology. The images acquired in this study provide information on tissue architectural morphology that could only previously be obtained with conventional biopsy. These results suggest that OCT may become a powerful imaging technology, enabling high-resolution diagnostic images, or optical biopsies, to be obtained for the purpose of detecting early stages of disease in the pancreatobiliary system.

ACKNOWLEDGMENTS

The contributions of E.A. Swanson of MIT Lincoln Laboratory are greatly appreciated. We also would like to thank J. Gamba and J. Taralli for their technical assistance.

REFERENCES

1. Botet JF, Lightdale C: Endoscopic ultrasonography of the upper gastrointestinal tract. Radiol Clin North Am 30:1067–1083, 1992
2. Nakaizumi A, Uehara H, Iishi H: Endoscopic ultrasonography in diagnosis and staging of pancreatic cancer. Dig Dis Sci 40:696–700, 1995
3. Hawes RH: New staging techniques: Endoscopic ultrasound. Cancer 71:4207–4213, 1993
4. Furukawa T, Tsukamoto Y, Naitoh Y: Evaluation of intraductal ultrasonography in the diagnosis of pancreatic cancer. Endoscopy 25:577–581, 1993
5. Furukawa T, Naitoh Y, Tsukamoto Y: New technique using intraductal ultrasound for diagnosis of diseases of the pancreatobiliary system. J Ultrasound Med 11:607–612, 1992
6. Huang D, Swanson EA, Lin CP, Schuman JS, Stinson WG, Chang W, Hee MR, Flotte T, Gregory K, Puliafito CA, Fujimoto JG: Optical coherence tomography. Science 254:1178–1181, 1991
7. Hee MR, Izatt JA, Swanson EA, Huang D, Lin CP, Shuman JS, Puliafito CA, Fujimoto JG: Optical coherence tomography of the human retina. Arch Ophthalmol 113:325–332, 1995
8. Puliafito CA, Hee MR, Lin CP, Reichel E, Shuman JS, Duker JS, Izatt JA, Swanson EA, Fujimoto JG: Imaging of macular diseases with optical coherence tomography. Ophthalmology 102:217–229, 1995
9. Schmitt JM, Knuttel A, Bonner RF: Measurements of optical properties of biological tissues by low-coherence reflectometry. Appl Opt 32:6032–6042, 1993
10. Schmitt JM, Knuttel A, Yadlowsky M, Eckhaus MA: Optical-coherence tomography of a dense tissue: Statistics of attenuation and backscattering. Phys Med Biol 39:1705–1720, 1994
11. Sergeev A, Gelikonov V, Gelikonov G: High-spatial-resolution optical-coherence tomography of human skin and mucous membranes. Conference on Lasers and Electro-Optics '95, paper CThN4, Optical Society of America, 1995
12. Fujimoto JG, Brezinski ME, Tearney GJ, Boppart SA, Bouma BE, Hee MR, Southern JF, Swanson EA: Biomedical imaging and optical biopsy using optical coherence tomography. Nature Med 1:970–972, 1995
13. Brezinski ME, Tearney GJ, Bouma BE, Izatt JA, Hee MR, Swanson EA, Southern JF, Fujimoto JG: Optical coherence tomography for optical biopsy: Properties and demonstration of vascular pathology. Circulation 93:1206–1213, 1996

14. Tearney GJ, Brezinski ME, Southern JF, Bouma BE, Boppart SA, Fujimoto JG: Optical biopsy in human gastrointestinal tissue using optical coherence tomography. Am J Gastroenterol 92:1800–1804, 1997
15. Swanson EA, Izatt JA, Hee MR, Huang D, Lin CP, Schuman JS, Puliafito CA, Fujimoto JG: *In vivo* retinal imaging by optical coherence tomography. Opt Lett 18:1864–1866, 1993
16. Tearney GJ, Brezinski ME, Bouma BE, Boppart SA, Pitris C, Southern JF, Fujimoto JG: *In vivo* endoscopic optical biopsy using optical coherence tomography. Science 276:2037–2039, 1997
17. Bouma B, Tearney GJ, Boppart SA, Hee MR, Brezinski ME, Fujimoto JG: High resolution optical coherence tomographic imaging using a mode-locked Ti:Al_2O_3 laser source. Opt Lett 20:1486–1488, 1995
18. Tearney GJ, Boppart SA, Bouma BE, Brezinski ME, Weissman NJ, Southern JF, Fujimoto JG: Scanning single mode fiber optic catheter/endoscope for optical coherence tomography. Opt Lett 21:543–545, 1995